ORIENTAL JOURNAL OF CHEMISTRY
An International Open Access, Peer Reviewed Research Journal
www.orientjchem.org
ISSN: 0970-020 X
CODEN: OJCHEG
2026, Vol. 42, No.(1):
Pg. 155-164

Synthesis and Benchmarking of $CH_3NH_3PbBr_3$ Perovskite Guided by the BR3 Framework for Green LED Applications

ZEINAB ABDALLAH MOHAMMED AHMED[1],NODAR KHALIFA[2], ALI A. S. MAROUF[3], MOHAMED ALZUBAIR ALMALEEH[4] and SHAL YASIN[5]

[1,2]Department of Physics, , Sudan University of Science and Technology, Khartoum, Sudan.
[3]Department of Engineering and Industrial Laser Application, Institute of Laser, Sudan.
[3]University of Science and Technology, Khartoum, Sudan.
[4]University of Technology& Applied Science- Rustaq, Oman.
[5]Sudanese Chemical Society, Sudan.
Email: sahlyasin@hotmail.com

http://dx.doi.org/10.13005/ojc/420116

(Received: June 28, 2025; Accepted: September 17, 2025)

ABSTRACT

Methylammonium lead bromide ($CH_3NH_3PbBr_3$) perovskite was synthesized via a solution-based route and systematically characterized to establish structure–morphology–property relationships. X-ray diffraction (XRD) confirmed a highly crystalline cubic phase, Fourier-transform infrared spectroscopy (FTIR) verified characteristic organic and inorganic vibrational modes, and scanning electron microscopy (SEM) revealed uniform, well-faceted grains, indicative of controlled crystal growth. By implementing the BR3 framework (Benchmarking, Refinement, Replication, Reporting), this study provides a reproducible, fully documented synthesis pathway that addresses the typical lack of rigorous structural and morphological benchmarking in $MAPbBr_3$ research. The resulting high-quality crystals demonstrate suitability for green-emitting optoelectronic devices, particularly LEDs, and establish a validated foundation for future device-focused optimization.

Keywords : Crystallite size, Methylammonium lead bromide ($MAPbBr_3$), Optoelectronic

INTRODUCTION

Hybrid organic–inorganic halide perovskites, with the general formula $CH_3NH_3PbX_3$ (X = I, Br, Cl), have emerged as a transformative class of semiconductors in solid-state physics and materials science. Their prominence arises from a highly adaptable crystal structure in which the organic cation (CH_3NH_{33}) is incorporated into an inorganic PbX_3 octahedral framework, combining the chemical versatility of organic molecules with the excellent charge-transport properties of inorganic semiconductors[1].

A defining feature of these materials is their tunable optoelectronic behavior. The bandgap of $CH_3NH_3PbX_3$

perovskites can be precisely tailored by varying the halide composition, typically spanning ~1.6 eV for X = I to ~2.3 eV for X = Br[2]. This ability to modulate absorption and emission spectra makes them highly attractive for a wide range of applications, including high-efficiency solar cells, bright light-emitting diodes (LEDs), and low-threshold lasers[3,4]. In addition, these perovskites exhibit strong optical absorption, long charge-carrier lifetimes, high mobility, and high photoluminescence quantum yields, properties that are critical for high-performance optoelectronic devices[3,5].

Despite their remarkable potential, translating laboratory-scale advances into reproducible, high-quality devices remains challenging. Variations in synthesis protocols can lead to inconsistencies in crystallinity, morphology, and optoelectronic performance, impeding reliable device fabrication[6]. Most studies focus on optical or device properties, while synthesis and structural–morphological benchmarking are treated as routine rather than systematically optimized. In particular, there is limited work that explicitly targets $MAPbBr_3$ as a green-light emitter, documents each synthesis step, correlates XRD, SEM, and FTIR results, and frames the material as a reproducible reference for future device studies. To address this gap, the present study applies the BR3 framework, Benchmarking, Refinement, Replication, and Reporting, to synthesize and comprehensively characterize $CH_3H_3PbBr_3$. This structured methodology enables reproducible production of high-crystallinity, phase-pure, morphology-controlled $MAPbBr_3$, explicitly positioned as a validated starting material for green perovskite LEDs and other optoelectronic applications.

EXPERIMENTAL

Materials and Synthesis

The following chemicals were used for synthesis without further purification: lead(II) acetate ($Pb(C_2H_3O_2)_3$, 99%), lead(II) nitrate ($Pb(NO_3)_2$, 99%), potassium bromide (KBr, 99.5%), potassium iodide (KI, 99%), methylamine solution (CH_3NH_3, 40% w/w in water), and hydrobromic acid (HBr, 48% w/w aqueous solution). The solvents N,N-dimethylformamide (DMF, analytical grade) and diethyl ether (analytical grade) were also used. Lead(II) bromide ($PbBr_2$, 99%) was used directly when commercially available; otherwise, it was synthesized in situ from $Pb(C_2H_3O_2)$ and KBr. The key physical and chemical properties of these reagents are summarized in Table 1. Other instruments and apparatus included 500-mL beakers, graduated cylinders, funnels, 250-mL conical flasks, an analytical balance, a water bath, a magnetic stirrer, a heating mantle, and filter paper.

Safety Note: All experiments involving lead compounds, hydrobromic acid, and methylamine were performed in a well-ventilated fume hood using standard personal protective equipment (lab coat, gloves, and safety goggles). Lead-containing waste and acidic residues were collected and disposed of

Table 1: Properties of the chemicals used for the synthesis of $CH_3NH_3PbBr_3$ perovskite

Compound	Formula	Molar mass ($g \cdot mol^{-1}$)	Density ($g \cdot cm^{-3}$)	Melting point (°C)	Purity / Concentration
Methylamine (aq.)	CH_3NH_2[3]	31.05	0.656	–93	40% (w/w) aqueous solution
Hydrobromic acid	HBr	80.91	1.49	–11	48% (w/w) aqueous solution
Potassium bromide	KBr	119.01	2.75	734	99.5% (purity)
Potassium iodide	KI	166.00	3.12	681	99% (purity)
Lead(II) acetate	$Pb(C_2H_3O_2)_3$	325.29	3.25	280	99% (purity)
Lead(II) nitrate	$Pb(NO_3)_2$[3]	331.20	4.53	470	99% (purity)
Lead(II) bromide *[1]	$PbBr_2$[3]	367.01	6.66	373	99% (purity)
N,N-Dimethylformamide	C_3H_7NO	73.09	0.944	–61	Analytical grade
Diethyl ether	$C_4H_{10}O$	74.12	0.713	–116	Analytical grade

in accordance with institutional hazardous waste management protocols to minimize health and environmental risks.

Method

All synthesis steps described below were conducted under the safety precautions to ensure safe handling of hazardous reagents. The procedures included the synthesis of methylammonium bromide (CH_3NH_3Br), lead(II) bromide, and the final organometallic halide perovskite $CH_3NH_3PbBr_3$. The characterization methods employed for product analysis are described in following:

Synthesis of Lead(II) Bromide ($PbBr_2$)

Lead(II) bromide was obtained via a precipitation reaction between lead(II) acetate [$Pb(C_2H_3O_2)_3$] and potassium bromide (KBr). In a typical procedure, an aqueous solution of $Pb(C_2H_3O_2)_2$ (0.1 mol, 32.5 g dissolved in 100 mL of water) was added dropwise to an aqueous solution containing a two-fold molar excess of KBr (0.2 mol) relative to $Pb^{2}{}_3$ to ensure complete precipitation of $PbBr_2$. A fine white precipitate of $PbBr_2$ formed immediately according to the double place reaction:

$Pb(C_2H_3O_2)_{2}{}_3(aq)+2KBr\ (aq)_3PbBr_2(s)+2K(C_2H_3O_2)$ (aq).. Eq(1)

The precipitate was collected by vacuum filtration, washed thoroughly with deionized water to remove residual potassium acetate, and dried at 60 °C for 24 h. Alternatively, high-purity commercial $PbBr_2$ (≥ 99%) was used directly.

Synthesis of Methylammonium Bromide (CH_3NH_3Br)

Methylammonium bromide was prepared by reacting methylamine solution (CH_3NH_2, 40% w/w, 0.3 mol, 38 mL) with an equimolar amount of hydrobromic acid (HBr, 48% w/w, 0.3 mol, ~34 mL) under ice-bath conditions to control the exothermic reaction. The mixture was stirred for two hours to yield a clear solution of CH_3NH_3Br. The solvent was evaporated to dryness at 60 °C, and the resulting crystalline solid was recrystallized from cold diethyl ether, filtered, and dried at room temperature for 120 h. The reaction is represented as:

$CH_3NH_{2(aq)} + HBr_{(aq)}\ \ CH_3NH_3Br_{(s)}$ .... Eq (2)

Synthesis of Organometallic Halide Perovskite Sensitizer ($CH_3NH_3PbBr_3$)

The organometallic halide perovskite $CH_3NH_3PbBr_{3}{}^3$ was synthesized by dissolving equimolar amounts of $CH_3NH_3Br_3$ and $PbBr_2$ (1:1 molar ratio, total ~2.84 g) in 20 mL of anhydrous DMF under continuous stirring at room temperature for two hours until a clear orange solution was obtained. Slow solvent evaporation yielded bright orange crystals of $CH_3NH_3PbBr_3$. The reaction can be expressed as:

$CH_3NH_3Br_{(s)}+\ PbBr_{3_{(s)}}\ \ (DMF)\ CH_3NH_3PbBr_3(aq)$ Eq (3)

Characterization

The synthesized $CH_3NH_3PbBr_{2}{}^3$ perovskite samples were characterized using complementary structural, morphological, and spectroscopic techniques. The crystal structure was examined using X-ray diffraction (XRD) to confirm phase formation, crystallinity, and lattice features. Surface morphology and grain texture were analyzed by scanning electron microscopy (SEM) at an accelerating voltage of 10.0 kV, with a view field of 136 µm, a working distance of 18.18 mm, and a magnification of approximately 1,020× (1.02 k×), using a secondary electron (SE) detector. Fourier-transform infrared (FTIR) spectroscopy was employed to identify characteristic vibrational modes and verify the incorporation of the methylammonium cation within the Pb–Br perovskite framework.

Implementation of the BR3 Framework

The synthesis process was structured and optimized according to the BR3 framework to ensure reproducibility and high material quality.

Benchmarking

Existing literature on precursor ratios, solvent selection, and crystallization conditions for $MAPbBr_3$ was comprehensively surveyed to establish a baseline synthesis protocol.

Refinement

Multiple repeated trial syntheses were performed, systematically adjusting parameters including solvent evaporation rate, precursor concentration, and stirring duration. This process

revealed that a controlled, slower solvent-evaporation rate was the most critical factor for achieving enhanced crystallinity and a larger, more uniform grain size.

Replication

The final optimized synthesis protocol, defined through the refinement stage, was reproduced in triplicate. The resulting samples showed consistent structural and morphological properties, with less than 3% variation in XRD peak intensity and SEM-observed grain morphology, confirming the robustness of the method.

Reporting

All synthesis steps, characterization procedures, and optimized parameters have been thoroughly documented in this work to promote reproducibility and facilitate further research.

This structured BR_3 approach was instrumental in consistently and reliably producing phase-pure, well-crystallized $MAPbBr_3$ material, as characterized in this study.

RESULTS AND DISCUSSION

X-Ray Diffraction XRD Structural Analysis

X-ray diffraction (XRD) was used to verify the crystal structure and phase purity of the synthesized $CH_3NH_3PbBr_3$ perovskite. The diffraction pattern in (Fig. 1) shows several sharp peaks within the 2θ range of 10°–18°, confirming the formation of a highly crystalline phase. The main reflections were recorded at 11.9°, 14.9°, and 17.0° match the expected fingerprint of cubic $CH_3NH_3PbBr_3$. The intense peak at 14.9° suggests a preferred orientation and high structural order.

The major peaks were indexed to the cubic perovskite structure and assigned to the (100), (110), and (200) planes, consistent with standard $MAPbBr_3$ reference patterns. These results confirm the successful synthesis of a phase-pure and well-crystallized $CH_3NH_3PbBr_3$ perovskite.

The XRD pattern of the synthesized $CH_3NH_3PbBr_3$ perovskite (Fig. 1) exhibits a dominant, sharp diffraction peak at 14.9°, corresponding to the (100) crystallographic plane of the cubic perovskite phase with Pm3m space group symmetry. This reflection is recognized in the literature as the primary fingerprint of cubic-phase $MAPbBr_3$ perovskite structure[13,14]. The sharpness and high intensity of the peak confirm excellent crystallinity and indicate high phase purity, as impurity or byproduct phases would introduce additional peaks of comparable intensity. Additional weaker reflections were observed near 11.9° and 12.6°, which may originate from low-index planes, residual precursor materials, or minor secondary phases; however, their negligible intensity relative to the 14.9° peak demonstrates that they do not compromise the

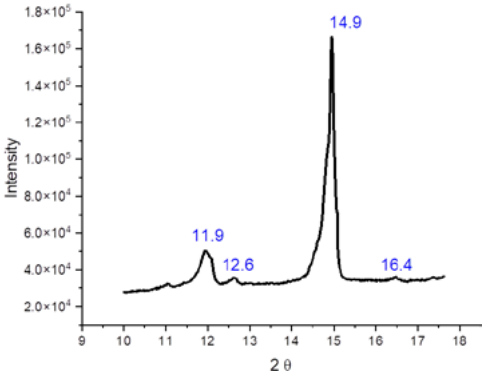

Fig. 1. XRD diffraction pattern of $CH_3NH_3PbBr_3$ perovskite showing characteristic peaks indexed to the cubic phase. Major reflections are assigned to the (100), (110), and (200) planes. The sharp and well-defined peaks indicate high crystallinity and phase purity of the synthesized material.

dominant cubic phase. These observations are consistent with previously reported XRD patterns for $CH_3NH_3PbBr_3$ perovskite, in which the cubic (100) reflection near 14.9° is consistently identified as the defining structural signature. While minor variations in peak intensity and low-angle features are known to arise from synthesis methods, sample thickness, or trace impurities, the persistence of the strong 14.9° peak in this work confirms the successful synthesis of highly crystalline and phase-pure cubic $CH_3NH_3PbBr_3$.

Crystallite Size Calculation

The crystallite size of the synthesized perovskite was calculated using the Scherrer equation

Where *D* demonstratedthe crystallite size, *K* is the shape factor (assumed to be 0.9), θ is the X-ray

wavelength (typically Cu *K*θ= 0.15406 nm), θis the full width at half maximum (FWHM, in radians), and θis the Bragg angle. The calculated values are summarized in Table 2.

The average crystallite size was found 314.07 nm, consistent with nanoscale crystalline domains characteristic of perovskite materials.

The calculated crystallite sizes are presented in Table 2. The obtained average crystallite size (~314 nm) aligns well with the nanocrystalline regime characteristic of perovskite materials.

Table 2: XRD peak parameters and crystallite

2θ (°)	**FWHM (°)**	**Crystallite Size (nm)**
11.944	0.34382	232.32
12.615	0.14548	549.40
14.915	0.26277	304.91
16.462	0.04676	171.66

The obtained average crystallite size (~314 nm) aligns well with previous studies on solution processed $MAPbBr_3$ perovskites, where crystallite sizes typically range from 200 to 400 nm, depending on the synthesis route and processing conditions[6,15,16]. Such values indicate well-developed nanocrystalline domains with excellent long-range order. Larger crystallite sizes are particularly beneficial for optoelectronic applications, as they reduce grain boundary density, minimize non-radiative recombination pathways, and enhance charge carrier transport. This is consistent with earlier findings that high-crystallinity $MAPbBr_3$ materials demonstrate superior photophysical properties and device performance in solar cells and light-emitting diodes[17-19].

In short, the Scherrer analysis confirms that the synthesized $CH_3NH_3PbBr_3$ perovskite possesses nanoscale crystallite domains of high quality, validating its structural suitability for advanced perovskite-based optoelectronic applications.

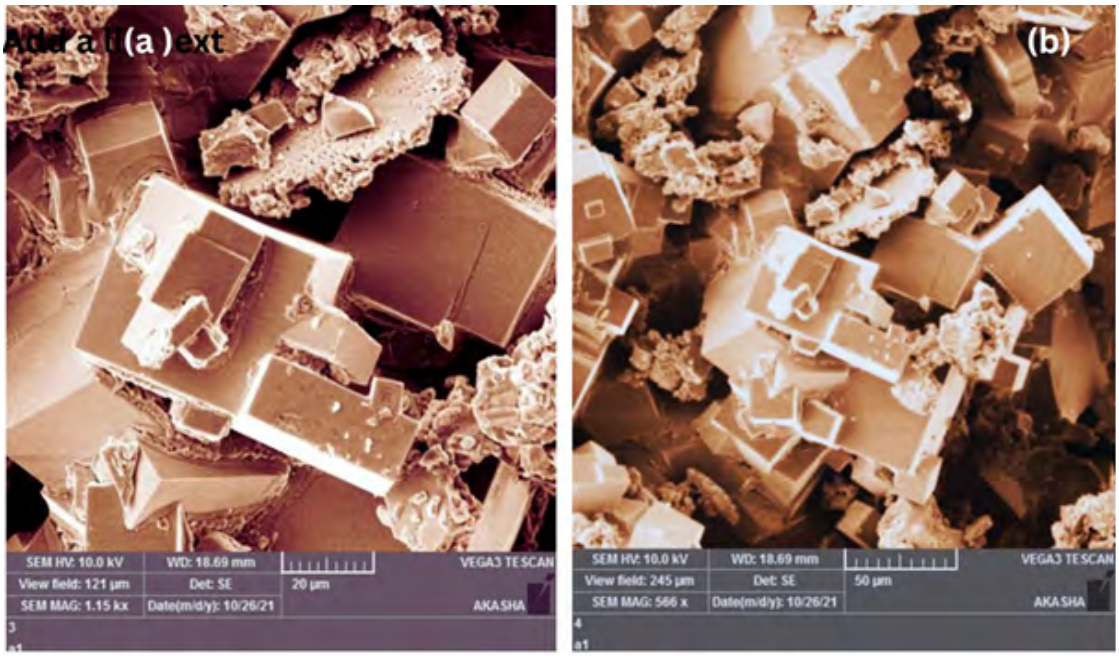

Fig. 2: SEM micrographs of $CH_3NH_3PbBr_3$ crystals at different magnifications. Clear embedded scale bars ((a) 20 *µ*m, and (b) 50 *µ*m respectively) are included within each image. The micrographs reveal well-defined cubic grains with uniform morphology, indicative of high-quality crystallization

SEM Morphology and Microstructure

Scanning electron microscopy (SEM) images (Fig. 2) confirmed the cubic grains characteristic of $CH_3NH_3PbBr_3$ crystals. The grains display clean facets and a relatively uniform size distribution, consistent with controlled nucleation

and growth during synthesis. Clear embedded scale bars (50 µm and 20 µm) are included directly in the images to ensure accurate interpretation of grain size and morphology.

The SEM micrograph of the synthesized $CH_3NH_3PbBr_3$ perovskite reveals well-defined, blocky microcrystals with sharp, faceted edges, a feature typical of high-quality methylammonium lead bromide prepared via solution-based methods. Numerous cuboid and plate-like crystals with distinct, flat faces are visible, indicating preferential growth along specific crystallographic directions, most likely the (001) plane, which is widely reported as a dominant growth facet for $MAPbBr_3$ in literature[15,20]. The relative uniformity in crystal shape suggests a controlled layered crystallization mechanism, in which cubes and plates are progressively formed by sequential layer deposition, consistent with previously observed growth pathways for hybrid perovskites[21-23].

The crystals appear interconnected, forming larger agglomerates while still maintaining their individual faceted structures, a hallmark of well-crystallized perovskite domains. The sharply defined geometries and the absence of rounded or amorphous particles confirm the high crystallinity and phase purity of the product, in agreement with the XRD results, which showed strong, single-phase reflections. Furthermore, the microcrystal surfaces appear relatively smooth, with minimal observable surface defects. Such high-quality surface morphology is desirable for optoelectronic applications, as it reduces the density of surface recombination centers that can otherwise limit charge-carrier lifetimes.

From the scale bar (20 µm), it is evident that some block crystals reach several micrometers in size. This observation is consistent with the XRD-derived average crystallite size of hundreds of nanometers, suggesting that the larger grains observed in SEM may result from the coalescence of smaller crystallites. Large grain domains are beneficial for device performance, as they reduce grain boundary density, enhance charge transport, and suppress trap-mediated recombination. The plate- and cube-like morphologies observed are also linked to uniform optical properties and reduced ion migration, which contribute to improved long-term stability of perovskite-based devices[24,25].

Overall, the SEM analysis confirms that the synthesized $CH_3NH_3PbBr_3$ perovskite demonstrates excellent crystalline quality, with well-faceted cubes and plates characteristic of optimal solution-processed growth. These morphological features are highly advantageous for photovoltaic and light-emitting applications, where grain size, crystallinity, and surfacesmoothness play critical roles in determining device efficiency and durability.

Fourier-Transform Infrared Spectroscopy

The FTIR spectrum of the synthesized $CH_3NH_3PbBr_3$ perovskite (Fig. 3) shows the characteristic vibrational modes of both the methylammonium cation and the Pb–Br inorganic lattice. A distinct band at 662.85 cm_3^1 is assigned to Pb–Br bending vibrations coupled with rocking motions of the MA_3 cation[7], confirming the formation of the coordinated Pb–Br framework. The mid-IR region displays several key features, including the MA_3 rocking mode at 929.08 cm_3^1, the C–N stretching vibration at 1018.62 cm_3^1, and the strong symmetric NH_3 bending mode at 1412.47 cm_3^1 with contributions from CH_3 deformation[8,9]. A sharper feature just below 1600 cm_3^1 corresponds to N–H bending, indicating the protonated state of the ammonium group and its hydrogen-bonding interaction with Br^- ions[9,10]. In the high-frequency region, the broad absorption centered near 3147.88 cm_3^1 is attributed to N–H stretching of the $–NH_{33}$ group, with the broadening reflecting the strong hydrogen-bonding network within the perovskite lattice[11,12]. A surrounding Br_3 ions, an interaction essential for stabilizing the hybrid perovskite lattice. The C–H stretching modes of the CH_3 group appear as well-defined peaks between 2800 and 3000 cm_3^1, confirming the incorporation of the organic cation. Vibrations observed between 1400 and 1600 cm_3^1 correspond to N–H bending modes, while a band near ~1000 cm_3^1 is assigned to C–N stretching, further verifying the structural integrity of the $CH_{33}NH_3$ ion.The absence of additional unassigned peaks suggests that the synthesized $CH_3NH_3PbBr_3$ is phase-pure and free from residual precursors or degradation products.

As expected for lead–halide perovskites, Pb–Br lattice vibrations occur below ~600 cm_3^1 and appear as weak low-wavenumber features due to

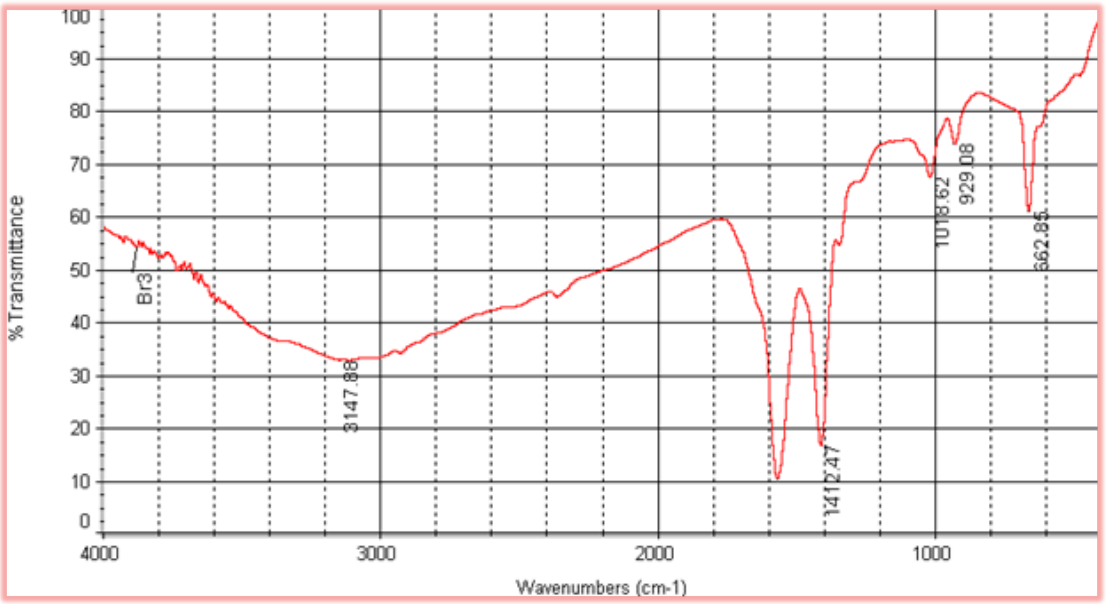

Fig. 3: FTIR spectrum of $CH_3NH_3PbBr_3$ showing characteristic vibrational bands

the limited sensitivity of standard mid-IR detectors in this region. Importantly, the absence of strong O–H stretching near 3200–3600 cm_3^1 indicates minimal moisture incorporation, a key factor in preventing degradation of hybrid halide perovskites. No additional bands attributable to precursor salts or solvent residues were detected, supporting the high purity of the synthesized material.

Furthermore, the FTIR spectrum provides clear evidence of intact organic–inorganic bonding, strong hydrogen-bonding interactions within the perovskite cage, and the absence of impurity signatures, all of which enhance the phase purity and structural stability inferred from XRD and SEM analyses.

The synthesized $CH_3NH_3PbBr_3$ perovskite exhibited high structural integrity and phase purity, as confirmed by XRD analysis, which revealed the expected cubic lattice without secondary phases. FTIR spectra confirmed the presence of characteristic organic–inorganic vibrational modes, while SEM imaging demonstrated well-defined grain morphology, indicative of uniform crystallization. Such structural coherence is crucial since morphological defects and secondary phases are known to compromise carrier transport and optical efficiency in perovskite-based devices.

The results establish a clear structure–property–application relationship: the synthesis method produces high-quality $CH_3NH_3PbBr_3$ with structural features known to support favorable optical behavior, highlighting its potential for next-generation optoelectronic devices. Further optimization of film thickness, interface engineering, and stability will be key to fully realizing this material's performance in solar cells, light-emitting diodes, and perovskite-based lasers.

Applications Supported by the Structural and Morphological Results

Perovskite-Based Green Light-Emitting Diodes (LEDs)

Among the potential applications of $CH_3NH_3PbBr_3$, the experimental results presented in this study most strongly support its use in green perovskite light-emitting diodes (LEDs). Several key findings align directly with the material requirements for high-performance emissive devices.

Alignment with Results

XRD and Crystallite Size:

The material exhibits high crystallinity with large nanoscale crystallites (average ≈ 314 nm). Such large grains reduce grain boundary density, suppress non-radiative recombination, and improve radiative efficiency, all critical factors for bright, stable LED emission.

SEM Morphology

The SEM micrographs display well-defined, faceted microcrystals with a relatively uniform size

distribution. This morphology facilitates smooth charge transport and minimizes leakage currents, supporting uniform and efficient electroluminescence.

FTIR Spectroscopy

FTIR analysis confirms the structural integrity of both the methylammonium cation and the Pb–Br framework. The absence of significant O–H bands indicates minimal moisture exposure, which is essential for operational stability in LED structures.

A Reliable Platform for Optoelectronic Device Prototyping and Fundamental Studies

Beyond specific device applications, the reproducibility and phase purity achieved in this synthesis make the material a valuable platform for exploring broader optoelectronic phenomena.

Alignment with Results

Integrated Structure–Property Relationship

The study demonstrates a clear link between synthesis parameters, crystallinity, and microstructure, confirming that the BR3-guided synthesis approach yields structurally reliable $CH_3NH_3PbBr_3$.

Reproducibility Across Techniques:

Consistent results from XRD, SEM, and FTIR confirm phase purity and stable organic–inorganic bonding. Such reproducibility is advantageous for: evaluating new device architectures, studying charge transport and recombination mechanisms, and benchmarking emerging perovskite compositions against a well-characterized reference material.

Limited Direct Support for Solar Cell Applications

Although $CH_3NH_3PbBr_3$ has recognized relevance in photovoltaic research, the present work does not include key photovoltaic characterization data, such as optical absorption spectra, optical bandgap determination, or electrical transport measurements, required to support solar-cell-oriented conclusions fully. Therefore, the applicability of solar cells cannot be strongly justified based solely on the reported XRD, SEM, and FTIR results.

Recommended Next Step: Development of a Green $CH_3NH_3PbBr_3$ LED Prototype

The structural and morphological quality demonstrated in this study provides a strong foundation for fabricating a green perovskite LED prototype. A simple device architecture may be adopted, such as:

ITO / Hole Transport Layer / $CH_3NH_3PbBr_3$ Emissive Layer / Electron Transport Layer / Metal Cathode

Future work should focus on

1. measuring the electroluminescence spectrum to verify green emission,
2. determining luminance and external quantum efficiency (EQE), and
3. evaluating operational stability under electrical bias.

Completing these steps would directly validate the practical viability of the synthesized $CH_3NH_3PbBr_3$ for LED applications.

The study demonstrates that the BR3 framework represents a methodological novelty by shifting $MAPbBr_3$ research from empirical synthesis toward a structured, reproducible, and benchmark-driven approach. Scientifically, the work goes beyond routine characterization by critically correlating controlled synthesis refinement with crystallinity, grain morphology, and organic–inorganic lattice integrity. The consistency across XRD, SEM, and FTIR results validates the framework's ability to reduce variability and establish $MAPbBr_3$ as a reliable reference material rather than a one-off synthesis outcome. This depth of analysis justifies the manuscript's contribution by positioning BR3 as a transferable strategy for improving rigor and reproducibility in perovskite materials research.

CONCLUSION

$CH_3NH_3PbBr_3$ perovskite was successfully synthesized via a solution-based route and systematically characterized by XRD, SEM, and FTIR. XRD confirmed a highly crystalline cubic phase, SEM revealed uniform, well-faceted grains, and FTIR verified characteristic organic and inorganic vibrational modes, demonstrating structural integrity and phase purity. These results establish a reproducible, high-quality $MAPbBr_3$ material suitable for green-emitting optoelectronic devices, particularly LEDs. Future work should focus on device fabrication, performance optimization, and stability studies to fully exploit the material's potential in practical applications.

ACKNOWLEDGMENT

The authors gratefully acknowledge the support and guidance received during the work. We extend our sincere appreciation toThe Sudanese Forensic Laboratoryfor providing laboratory facilities and technical assistance.

Conflict of interest: All authors declare that there are no conflicts of interest, whether financial, personal, or professional, that could have biased the research, analysis, or conclusions presented in this manuscript.

Author Contributions

Zeinab Abdallah conceptualization and writing original draft preparation; Nodar Osman; formal analysis. Ali A. S; draft preparation Sahl Yasin, and Mohamed Alzubair, review, and editing.

Data Availability Statement

The data are available from the corresponding author upon reasonable request.

REFERENCES

1. Zhao Y, Zhu K. Organic–inorganic hybrid lead halide perovskites for optoelectronic and electronic applications. Chemical Society Reviews. **2016**;45(3):655-89.DOI https://doi.org/10.1039/C4CS00458B
2. Sutter-Fella CM, Li Y, Cefarin N, Buckley A, Ngo QP, Javey A, Sharp ID, Toma FM. Low Pressure Vapor-assisted Solution Process for Tunable Band Gap Pinhole-free Methylammonium Lead Halide Perovskite Films. Journal of Visualized Experiments: Jove. 2017 Sep 8(127):55404.htpp://doi:2010.3791/55404
3. Tyagi D, Laxmi V, Basu N, Reddy L, Tian Y, Ouyang Z, Nayak PK. Recent advances in two-dimensional perovskite materials for light-emitting diodes. Discover Nano. 2024 Jul 2;19(1):109.https://doi.org/10.1186/s11671-024-04044-2
4. Xing G, Mathews N, Lim SS, Yantara N, Liu X, Sabba D, Grätzel M, Mhaisalkar S, Sum TC. Low-temperature solution-processed wavelength-tunable perovskites for lasing. Nature materials. **2014** May;13(5):476-80. https://doi.org/10.1038/nmat3911
5. Aftab S, Kabir F, Mukhtar M, Hussain I, Nazir G, Aslam M, Hegazy HH, Yewale MA. Perovskite quantum wires: A review of their exceptional optoelectronic properties and diverse applications in revolutionary technologies. *Nano Energy*. **2024** Oct 1;129:109995.https://doi.org/10.1016/j.nanoen.2024.109995
6. Seyisi T, Fouda-Mbanga BG, Mnyango JI, Nthwane YB, Nyoni B, Mhlanga S, Hlangothi SP, Tywabi-Ngeva Z. Major challenges for commercialization of perovskite solar cells: A critical review. *Energy Reports.* **2025** Jun 1;13:1400-15.https://doi.org/10.1016/j.egyr.2025.01.019
7. Zhang F, Karimata I, Wang HW, Tachikawa T, Tominaga K, Hayashi M, Sasaki T. Terahertz spectroscopic measurements and solid-state density functional calculations on CH3NH3PbBr3 perovskites: Short-range order of methylammonium. *The Journal of Physical Chemistry C.* **2021** Dec 29;126(1):339-48.https://doi.org/10.1021/acs.jpcc.1c06988
8. Panneerselvam V, Salammal ST, Chinnakutti KK, Manidurai P. Vibrational modes, chemical states and thermal stability of mechanochemically synthesized methylammonium lead iodide (CH3NH3PbI3) perovskites. Materials Letters. **2019** Apr 15;241:140-3.https://doi.org/10.1016/j.matlet.2019.01.069
9. Pérez-Osorio MA, Lin Q, Phillips RT, Milot RL, Herz LM, Johnston MB, Giustino F. Raman Spectrum of the Organic–Inorganic Halide Perovskite $CH_3NH_3PbI_3$ from First Principles and High-Resolution Low-Temperature Raman Measurements.https://doi.org/10.1021/acs.jpcc.8b04669
10. Feliciano GT. Vibrational properties of the organic-inorganic halide perovskite $CH_3NH_3PbI_3$ from theory and experiment: factor group analysis, first-principles

calculations, and low-temperature infrared spectra [dissertation]. São Paulo: Universidade de São Paulo; **2015**. doi: 10.11606/D.43.2015.tde-20102015-145926.

11. Hansen PE, Vakili M, Kamounah FS, Spanget-Larsen J. NH stretching frequencies of intramolecularly hydrogen-bonded systems: an experimental and theoretical study. Molecules. **2021** Dec 17;26(24):7651. Anikeeva, V.E., Boldyrev, K.N., Semenova, O.I., Sukhikh, T.S. and Popova, M.N., 2023. Broad-range high-resolution optical spectroscopy of $CH_3NH_3PbBr_3$ hybrid perovskite single crystals: Optical phonons, absorption edge, phase transitions. *Optical Materials*: X, 20, p.100259. https://doi.org/10.3390/molecules26247651
12. Hussain S, Khan MI, Subhani WS, Mustafa GM, Saleem M, Abubshait SA, Abubshait HA, Saleh DI, Mahmoud SF. Decorating wide band gap $CH_3NH_3PbBr_3$ perovskite with 4AMP for highly efficient and enhanced open circuit voltage perovskite solar cells. *Solar Energy.* **2021** Dec 1;230:501-8. Gidey, A.T., Haruta, Y., Herman, A.P., Grodzicki, M., Melnychenko, A.M., Majchrzak, D., Mahato, S., Rogowicz, E., Syperek, M., Kudrawiec, R. and Saidaminov, M.I., **2023**. Surface Engineering of Methylammonium Lead Bromide Perovskite Crystals for Enhanced X-ray Detection. *The Journal of Physical Chemistry Letters,* 14(40), pp.9136-9144. https://doi.org/10.1016/j.solener.2021.10.01
13. Heindl MW, Lichtenegger MF, Kodalle T, Liu S, Solhtalab N, Zerhoch J, Shcherbakov A, Kivala M, Sutter3Fella CM, Urban AS, Deschler F. Ligand3Induced Crystallization Control in $MAPbBr_3$ Hybrid Perovskites for High Quality Nanostructured Films. *Advanced Optical Materials.* **2025** Feb;13(6):2402441. https://doi.org/10.1002/adom.202402441
14. Zhao T, Guo Y, Yang X, Xiong Q, Gao P, Meng L, Xiong Z. Pure 3-phase (FAPbI3) 0.83 (MAPbBr3) 0.17 powder for efficient perovskite solar cells with enhancing reproducibility. *Materials Today Communications.* **2024** Dec 1;41:110398.https://doi.org/10.1016/j.mtcomm.2024.110398
15. slam MJ, Islam MH. Tuning emission and bandgap dynamics of $MAPbBr_3$ single crystals through halide exchange with methyl iodide. *Chemical Physics Impact.* **2025** Jun 1;10:100807.https://doi.org/10.1016/j.chphi.2024.100807
16. Mahato S, Makowski M, Bose S, Kowal D, Kuddus Sheikh MA, Braueninger-Wemer P, Witkowski ME, Ray SK, Drozdowski W, Birowosuto MD. Improvement of light output of MAPbBr3 single crystal for ultrafast and bright cryogenic scintillator. *The Journal of Physical Chemistry Letters.* **2024** Mar 28;15(14):3713-20.https://doi.org/10.1021/acs.jpclett.4c00379
17. Vila M, Bartolomé J, El Astal-Quirós A, Martínez-Pastor JP, Suarez I, de Andrés A, Coya C. Morphology engineering of MAPbBr3 thin films for enhanced lighting applications. *APL Materials.* **2025** Jul 1;13(7).https://doi.org/10.1063/5.0263289
18. Cho Y, Jung HR, Jo W. Halide perovskite single crystals: growth, characterization, and stability for optoelectronic applications. *Nanoscale.* **2022**;14(26):9248-77.https://DOI:10.1039/D2NR00513A
19. Bonadio A, Souza JA. Hybrid MAPbI 3 Perovskite Growth Mechanism from Irregular Particles to Cuboid and Hopper-Type Morphologies. *Journal of the Brazilian Chemical Society.* **2022** Oct 24;33:1273-80. https://doi.org/10.21577/0103-5053.20220057
20. Gao Q, Fang H, Xiang D, Chen Y, Tanaka H, Tan P. Impact of impurities on crystal growth. *Nature Physics.* **2025** Apr 15:1-9. https://doi.org/10.1038/s41567-025-02870-4
21. O'Brien MN, Jones MR, Mirkin CA. The nature and implications of uniformity in the hierarchical organization of nanomaterials. *Proceedings of the National Academy of Sciences.* **2016** Oct 18;113(42):11717-25. https://doi.org/10.1073/pnas.1605289113
22. Wang S, Frisch S, Zhang H, Yildiz O, Mandal M, Ugur N, Jeong B, Ramanan C, Andrienko D, Wang HI, Bonn M. Grain engineering for improved charge carrier transport in two-dimensional lead-free perovskite field-effect transistors. *Materials Horizons.* **2022**;9(10):2633-43.https://DOI:10.1039/D2MH00632D